ERRATUM PUBLISHED 18 DECEMBER 2024; SEE LAST PAGE

PROSTHETICS

Restoration of grasping in an upper limb amputee using the myokinetic prosthesis with implanted magnets

Marta Gherardini[1,2]†, Valerio Ianniciello[1,2]†, Federico Masiero[1,2], Flavia Paggetti[1,2], Daniele D'Accolti[1,2], Eliana La Frazia[1,2], Olimpia Mani[3], Stefania Dalise[4], Katarina Dejanovic[1,2], Noemi Fragapane[4], Luca Maggiani[4], Edoardo Ipponi[3], Marco Controzzi[1,2], Manuela Nicastro[5], Carmelo Chisari[4], Lorenzo Andreani[3], Christian Cipriani[1,2]*

The loss of a hand disrupts the sophisticated neural pathways between the brain and the hand, severely affecting the level of independence of the patient and the ability to carry out daily work and social activities. Recent years have witnessed a rapid evolution of surgical techniques and technologies aimed at restoring dexterous motor functions akin to those of the human hand through bionic solutions, mainly relying on probing of electrical signals from the residual nerves and muscles. Here, we report the clinical implementation of an interface aimed at achieving this goal by exploiting muscle deformation, sensed through passive magnetic implants: the myokinetic interface. One participant with a transradial amputation received an implantation of six permanent magnets in three muscles of the residual limb. A truly self-contained myokinetic prosthetic arm embedding all hardware components and the battery within the prosthetic socket was developed. By retrieving muscle deformation caused by voluntary contraction through magnet localization, we were able to control in real time a dexterous robotic hand following both a direct control strategy and a pattern recognition approach. In just 6 weeks, the participant successfully completed a series of functional tests, achieving scores similar to those achieved when using myoelectric controllers, a standard-of-care solution, with comparable physical and mental workloads. This experience raised conceptual and technical limits of the interface, which nevertheless pave the way for further investigations in a partially unexplored field. This study also demonstrates a viable possibility for intuitively interfacing humans with robotic technologies.

INTRODUCTION

People affected by hand amputation suffer severe consequences in terms of physical and psychological well-being as a result of substantial functional impairments and major changes in social life. To help them regain the lost functionality, bioengineers are searching for a human-machine interface (HMI) that allows real-time, parallel, direct, and simultaneous control over multiple degrees of freedom (DoFs) of an artificial limb in a physiologically appropriate manner as well as a bidirectional flow of information. Machine learning algorithms applied to surface electromyography (EMG) signals, developed by researchers for more than 50 years, are currently the most technologically advanced control solution clinically available (*1*, *2*). Although clinically available technologies lack the restoration of highly dexterous motor skills equivalent to those of the human hand, a new spectrum of opportunities aimed at filling this gap is being explored by researchers. Advanced surgical techniques to uncover concealed control sources and develop mechanically stable attachments of the prosthesis, combined with highly selective probing technologies and advanced control algorithms, are paving the way for the bionic reconstruction of amputated limbs (*3*, *4*).

Most of the control and sensory feedback strategies available or proposed so far rely on the transduction/encoding of efferent/afferent electrical signals from/to the brain, exploiting the peripheral physiological structures (nerves and muscles) (*5*–*12*). We propose an alternative HMI that takes advantage of the physical displacement undergone by skeletal muscles during contraction to decode the user's intention. We named it the myokinetic interface (*13*, *14*). The core of the interface is a multitude of permanent magnets implanted through a minimally invasive procedure into the residual muscles. Magnet displacement induced by muscle contraction and retrieved through a transcutaneous magnet localizer (TML) is translated in a driving signal for the prosthesis (the myokinetic control interface). The myokinetic interface is based on implantable technologies, but the implanted devices do not require wireless powering or percutaneous wires. Compared with fully implantable electromyographic sensors, such as the implantable myoelectric sensors (IMESs) system (*11*), magnets exhibit reduced dimensions and, unlike IMES, which are sensors de facto, could serve as bidirectional communication channels (*15*). Whereas muscle electrical activity provides only an indirect measure of muscle force (*16*), magnets could enable a direct measure of muscle length and velocity, allowing accurate correlation of muscle activation to muscle force (*17*). Another notable solution proposed by Cederna and colleagues (*12*) is the surgical creation of nerve amplifiers consisting of small muscle grafts, regenerative peripheral nerve interfaces (RPNIs). Percutaneous electrodes are currently used to record the EMG signals from RPNIs, yet they historically suffer from safety and reliability issues that compromise their long-term stability (*18*). Thus, RPNIs could benefit from the

[1]BioRobotics Institute, Scuola Superiore Sant'Anna, Pisa, Italy. [2]Department of Excellence in Robotics and AI, Scuola Superiore Sant'Anna, Pisa, Italy. [3]Orthopaedics and Traumatology Unit, University Hospital of Pisa, Pisa, Italy. [4]Neurorehabilitation Unit, University Hospital of Pisa, Pisa, Italy. [5]Orthopaedic and Burn Centre Anaesthesiology and Reanimation, University Hospital of Pisa, Pisa, Italy.
*Corresponding author. Email: christian.cipriani@santannapisa.it
†These authors contributed equally to this work.

development of wireless probing technologies suitable for integration inside their restrained volume. Although applicable to all forms of limb amputations, the myokinetic interface finds its most suitable clinical and scientific application in the treatment of transradial amputations, because magnets implanted in several extrinsic muscles of the forearm could potentially restore the noteworthy dexterity of hand movements. For the past 8 years, we extensively investigated the theoretical feasibility (*14*, *19*–*22*) and developed the enabling technologies for myokinetic control (*23*, *24*).

Here, we present a first-in-human demonstration of the myokinetic control interface controlling a self-contained prosthetic arm, in a transradial amputee, through a 6-week study. The outcomes from this pilot study were promising given its short duration: The participant was able to complete a series of functional tests, achieving a performance comparable to that achieved using myoelectric controllers, a standard-of-care solution. Nevertheless, this experience also galvanizes further studies on the biomechanics of muscle contraction and tissue deformation; on the conceptual and technical limits of the proposed HMI, including its surgical implementation; and on the solutions to overcome them.

RESULTS

Clinical implementation

The participant was amputated at the distal third of the left forearm (nondominant side) after a traumatic event that had occurred 5 months before their enrollment and started using a myoelectric prosthesis 1 month before receiving the implant. Preliminary clinical assessments (ultrasound imaging and needle EMG) ensured the absence of moderate to severe degrees of muscle fibrosis in nine forearm muscles and allowed us to identify the optimal set of muscles to receive the implants on the basis of the observed displacement and muscle function in addition to ease of insertion. The participant could activate the digits of the phantom hand, as confirmed by corresponding activations in the extrinsic muscles observed with ultrasound. Six cylindrical (2-mm radius and height), axially magnetized neodymium magnets coated with medical-grade parylene C were implanted in three target muscles (two magnets per muscle), namely, the flexor carpi ulnaris (FCU), the extensor digitorum (ED), and the flexor pollicis longus (FPL) (Fig. 1). Before surgery, target muscle sites were marked with a skin pen under ultrasound guidance while the participant was asked to activate each muscle. The surgical procedure was performed under local anesthesia and deep sedation in the operating theater. The magnets were inserted in pairs per muscle belly, in the proximal (FCU_p, ED_p, and FPL_p) and distal (FCU_d, ED_d, and FPL_d) portion of the muscle, and were separated by a minimum distance of 3 cm to prevent migration because of magnetic attraction/repulsion. Small incisions less than 2 cm were performed on the target sites. Nonmagnetic tweezers were used to manipulate the magnets, which were implanted in the target site enclosed in a cube of Spongostan, an absorbable hemostatic gelatin sponge used to control bleeding during surgical procedures, to minimize the surrounding tissue reaction and mobilization. The implantation site in the target muscle was verified under ultrasound sterile guidance. Fibrin sealant was injected at the implant site, and intradermal suturing with absorbable threads was performed on the skin incision. Wounds were covered with a standard bandage and were desutured on the 10th postoperative day. The entire surgical procedure (from incision to sutures) lasted for 1.5 hours. Periodic ultrasound imaging throughout the implantation period (10 repetitions of three different movements) was used to monitor the displacement of single magnets over time. The latter revealed a stable average displacement of 0.5 and 1 mm, in FPL_p and FPL_d, respectively, induced by thumb flexion, in both the longitudinal and transverse muscle plane (Fig. 1, A and B). An average displacement of 1 mm was induced by ulnar deviation on FCU_p (longitudinally and transversely) and FCU_d (longitudinally), whereas an average displacement of 0.5 mm was measured for FCU_d in the transverse plane. The extension of the four digits led to a marginal increase in displacement in ED_p and ED_d in the weeks after implantation, ultimately reaching an average value >1 mm.

Because these measures were restricted to a two-dimensional (2D) space, a complete description of the magnet displacement could only be derived from the localization output, which showed a maximum displacement above 6 mm achieved by FPL_d during wrist supination (fig. S1). During the 6 weeks, the pain associated with the phantom limb (*R* score) increased from ~8 before surgery to ~10 after surgery but gradually decreased to a score of ~5 at completion of the study, according to the McGill Pain Questionnaire (*25*). The participant described the pattern of pain as "continuous" and the phantom limb as "telescoping." The participant could only feel the magnets by pressing on the skin with the nonamputated hand, experiencing no discernible presence or discomfort from the implants otherwise. The participant seamlessly continued to use his myoelectric prosthesis at home during the whole implantation period.

After 6 weeks, the magnets were explanted in the theater under local anesthesia and deep sedation. Surgical access areas were even smaller than those performed for the implantation procedure because the magnets did not migrate from the implantation site. Magnets were removed under ultrasound intraoperative guidance. Intradermal suturing with absorbable threads was performed. The duration of the explant was 1.5 hours. The magnets did not cause any type of reaction in the surrounding tissues, with the exception of one that had not retained the Spongostan wrap around it. Intraoperative biopsy of a small piece of reactive tissue was performed, and the anatomical-pathological result confirmed a low-grade granulomatous inflammation. The remaining tissues were healthy.

Signal characterization

Candidate control inputs for the myokinetic controller were variations of the poses (position and orientation) relative to each pair of magnets, from the relaxed to the contracted state in the muscles (contraction shift). These control inputs were retrieved by sampling the magnetic field produced by the magnets, using a grid of 140 sensors distributed over the implantation sites within a prosthetic socket, and solving the inverse problem of magnetostatics (*14*).

A real-time tracking task aimed to assess the dynamic performance of the HMI and quantify the effective independence of the implanted muscles demonstrated, however, an imperfect separability of the three myokinetic channels (Fig. 1C). When the participant was instructed to perform nonfatiguing movements corresponding to a prevalent activation of each of the three implanted muscles (FCU, FPL, and ED), only the contraction shifts associated with FCU (~1 mm median) and FPL (~2.6 mm) were independent, with the elbow extended. However, such a pattern could not be observed when the elbow was flexed. The flexion/extension of the elbow also affected the absolute pose of the magnets and the distance between all pairs of magnets in the relaxed state of the muscles (Fig. 1D). For example, when going from 0° to 70° of elbow flexion, the distance at rest (relaxed muscle state) between FPL_p and FPL_d decreased by ~2 mm, whereas for ED, it decreased by a maximum of ~12 mm (Fig. 1D).

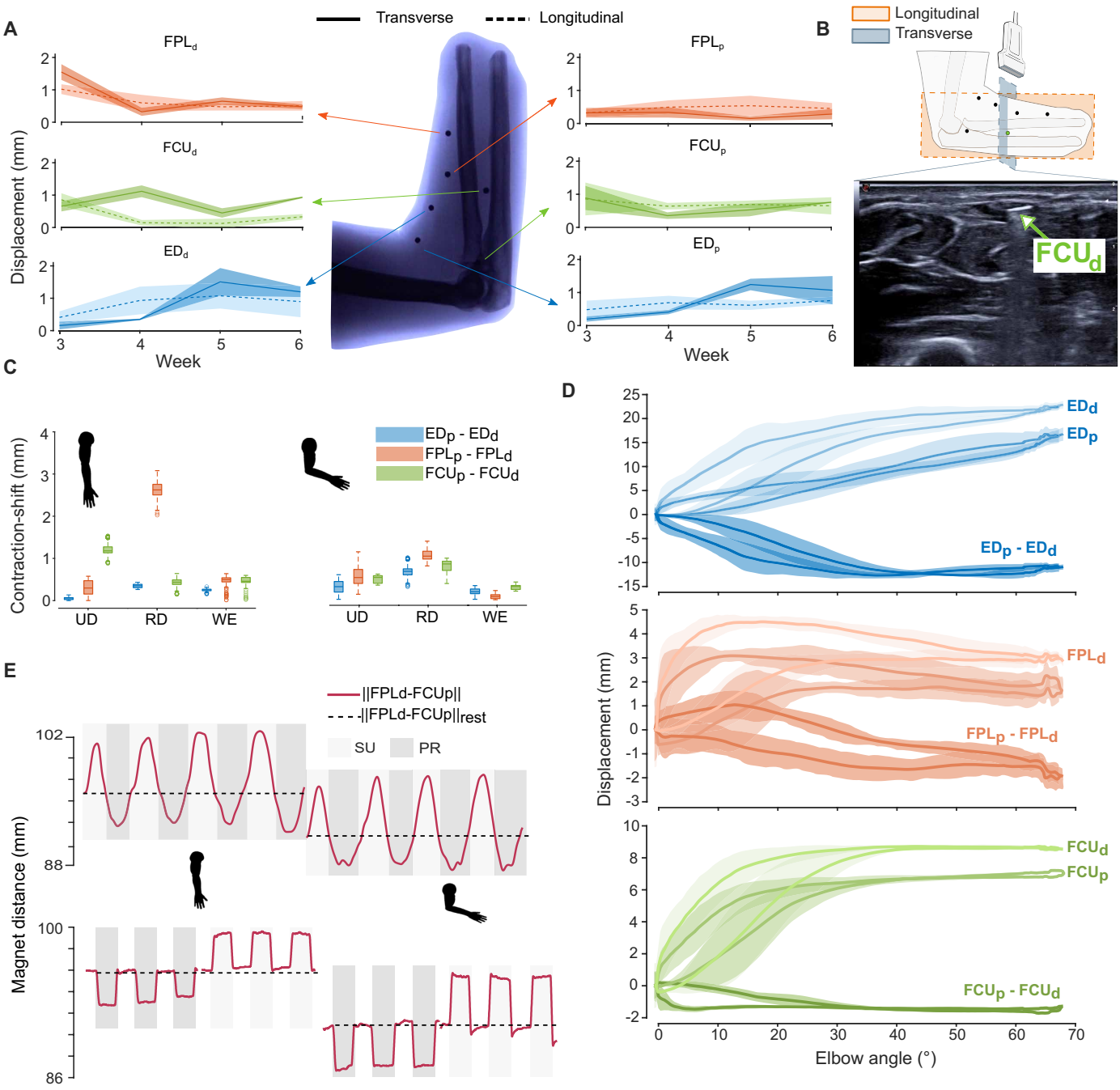

Fig. 1. Clinical implementation and signal characterization. (**A**) Mean (solid/dashed lines) and SD (shaded area, 10 repetitions) of the displacement of each magnet from its position at rest prevalent activation of each of the three implanted muscles (namely, thumb flexion for the FPL, ulnar deviation for the FCU, and four-digit extension for the ED, derived through periodic ultrasound imaging throughout the implantation period). Stable patterns of displacement were found both in the longitudinal and the transverse muscle plane. (**B**) Example frame extracted from a video acquired with the ultrasound probe in the transverse plane of the FCU. The frame captures the magnet implanted distally in the muscle. (**C**) The boxplots represent the contraction shifts relative to each magnet pair in the same muscle, caused by ulnar deviation (UD), radial deviation (RD), and wrist extension (WE), with both extended and flexed elbow. Boxplots contain data extracted from three repetition of each movement, discarding the transient. (**D**) Mean (solid line) and SD (shaded area) of the displacement for each magnet (variation from the position at rest), and between each magnet pair in the same muscle (variation from their distance at rest), caused by elbow flexion/extension. Specifically, rest refers to the position of the individual magnets (distance between magnet pairs) corresponding to 0° of elbow flexion. Curves were derived from five repetitions of elbow flexion/extension performed by the participant while matching three different sinusoidal waves (6-, 4-, and 3-s periods). (**E**) Distance between FPL_d and FCU_p while matching sinusoidal waves (above) and sequences of steps (below) by performing wrist pronation and supination, with both extended and flexed elbow. The graphs show that the distance at rest between the magnets was affected by the elbow movement (dashed line).

On the contrary, wrist pronation and supination movements captured using the poses from FPL_d and FCU_p demonstrated a high degree of controllability, because the participant could finely modulate the signal when matching sinusoidal waveforms on a PC screen (Fig. 1E). These signals also demonstrated a good signal-to-noise ratio (SNR), given that the contraction shifts associated with voluntary contractions were considerably larger than those observed in other magnet pairs (Fig. 1, C and E). Last, these signals showed good robustness against elbow angle, because similar contraction shifts were observed at different elbow angles (Fig. 1E). For example, when the participant supinated the wrist at ~50% maximum voluntary contraction, a maximum contraction shift of 3 mm was measured with the elbow extended, whereas a maximum of 4.5 mm was reached with the elbow flexed at 80°.

These patterns were stable throughout the 6-week period, showing no significant linear or monotonic trend, in agreement with the outcomes of the periodic ultrasound measures (fig. S1). Stability was also confirmed by the absence of notable patterns resulting from voluntary contraction or elbow movement throughout the implantation period.

Self-contained prosthetic hand

We developed a self-contained prosthetic hand that integrated all the functional components, including a TML, battery, robotic hand, and self-suspending socket (Fig. 2). As anticipated, the TML retrieved the poses of the implanted magnets, via numerical solving methods fed with the magnetic field sampled by a grid of 140 sensors distributed over the implantation sites, within the socket. The poses of the magnets were thus used as inputs for a control system [either a speed direct controller or a pattern recognition controller (*26*)], also implemented in the TML, that decoded the user's intention by sending the appropriate commands to the hand.

For comparison with standard-of-care solutions, the week before the surgery, we fitted the participant with a two-state amplitude modulated myoelectric controller and administered the same functional tests used to evaluate the prosthesis under myokinetic control. For the hand, we used the Mia research hand (by Prensilia Srl), an instrumented, human-sized, multi-articulated, versatile robotic hand that enabled palmar, precision, and lateral grasps.

Direct control

The characterization of the signals helped create a model for an optimized direct control strategy, finely tuned to the observed contraction shifts and artifacts caused by elbow flexion. According to this model, the TML mapped the contraction shift induced between FPL_d and FCU_p during supination and pronation of the wrist to the opening and closing of the robotic hand, respectively (Fig. 3A). Because FPL_d and FCU_p got closer during supination and moved away during pronation, a positive and a negative thresholds were set to detect the participant's intention to open and close the hand, respectively. The control input granularly captured the degree of muscle contraction (Fig. 1A), and thus proportional control could be implemented by linear mapping to the corresponding speed of hand opening/closing. Once the target position was reached, it was maintained without the requirement to keep muscle contraction.

To avoid unwanted hand activations because of elbow artifacts, we implemented an enable/disable switch by setting a threshold on the slope of the distance at rest between ED_p and ED_d; in other words, no drive signal could be sent to the hand if this threshold was exceeded (Fig. 3B). New control inputs were reenabled after the slope remained below the threshold for at least 400 ms.

Pattern recognition

The TML used a three-class (hand opening, hand closing, and resting) pattern recognition controller using linear support vector machines

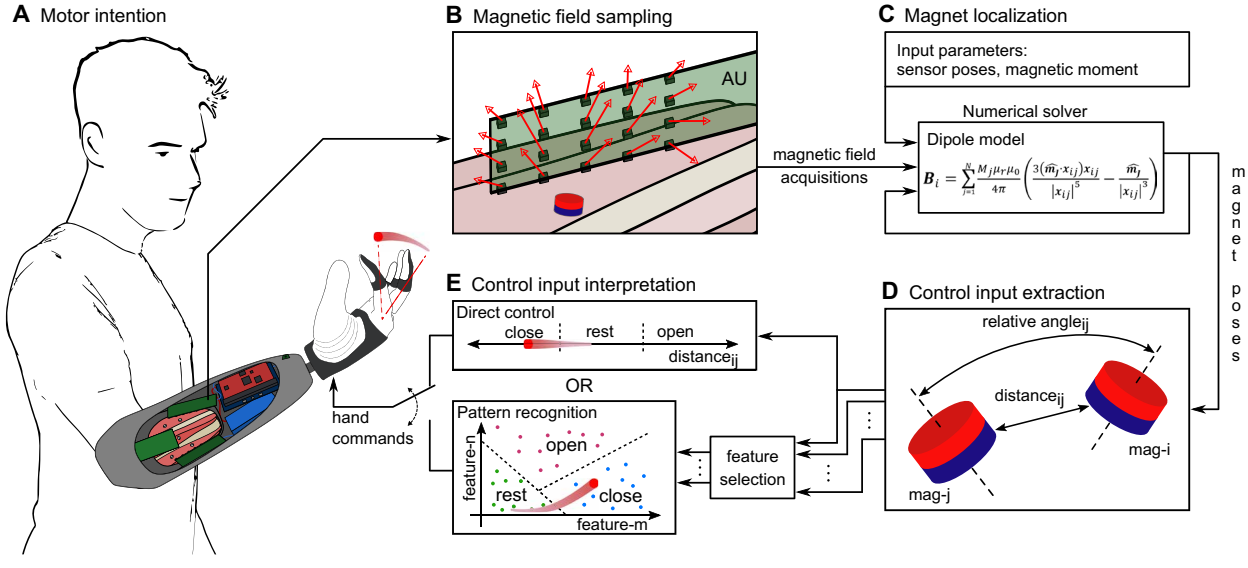

Fig. 2. The myokinetic prosthetic hand. (**A**) The user's motor intention travels from the brain to the muscles through the efferent neural pathways, inducing muscle deformation. (**B**) Magnetic field sensors sample the magnetic field generated by the implanted magnets and transmit the acquisitions to an embedded computing unit. (**C**) An iterative numerical solver retrieves the poses (position and orientation) of the six magnets by modeling the sensed magnetic field as a superimposition of magnetic dipoles. (**D**) The candidate control inputs are computed from the retrieved poses as the distances and relative angles between all magnet pairs. (**E**) The control inputs are interpreted through a direct or pattern recognition control strategy and translated into commands for the robotic hand.

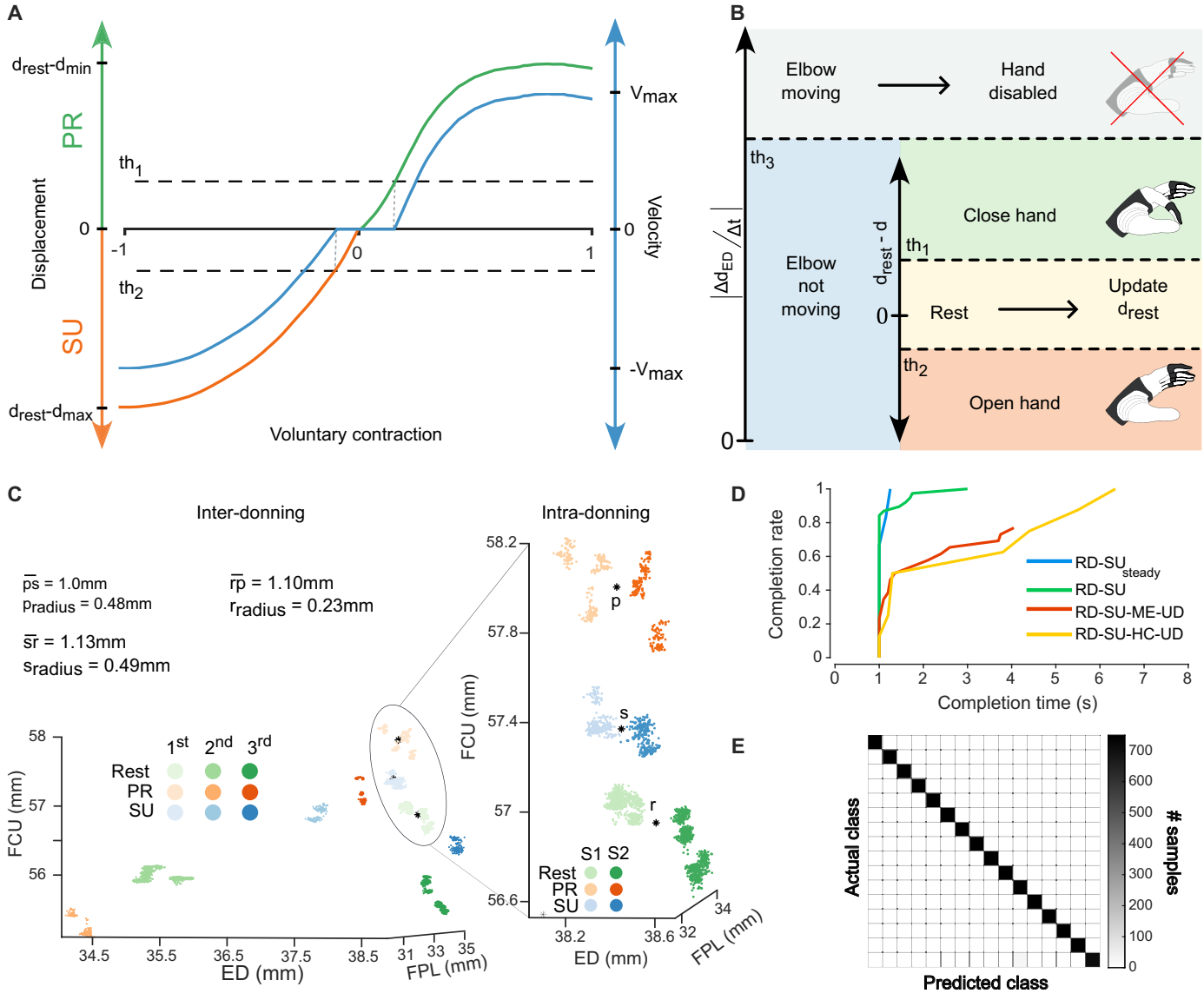

Fig. 3. Direct control signals and workflow and pattern recognition training data, online and offline results. (**A**) The contraction shift between FPL_d and FCU_p ($d_{rest} - d$) during supination (SU) and pronation (PR) of the wrist was mapped to the opening ($d_{rest} - d < th_2$) and closing ($d_{rest} - d > th_1$) of the robotic hand. Proportional control was implemented by linear mapping to the corresponding speed of the robotic hand. (**B**) Direct control strategy. An enable/disable switch was implemented by setting a threshold, th_3, on the slope of the distance at rest between ED_p and ED_d ($\Delta d_{ED}/\Delta t$), to counteract elbow artifacts. If the elbow was not moving ($\Delta d_{ED}/\Delta t < th_3$), direct control was implemented according to (A). *d* indicates distance; *V*, velocity; and *t*, time. (**C**) In intradonning data, contraction patterns related to PR, SU, and rest resulted in linearly separable clusters in terms of distances between magnet pairs. This held true across multiple sessions (S1 and S2), that is, across acquisitions performed before and after asking the participant to repeatedly move the elbow. On the contrary, cluster separation was unstable across multiple donnings. Dots represent samples derived from the steady-state phase of 5-s contractions, repeated three times per movement. (**D**) The motion test had completion rates of 100% when the SVM was trained to discriminate RD and SU, both with the arm in a fixed position ($RD\text{-}SU_{steady}$) and with the arm reaching six different target positions (RD-SU). In this latter case, when retrained with two sets of five classes (RD-SU-ME-UD and RD-SU-HC-UD, where ME is middle finger extension and HC is hand closing), the SVM yielded completion rates of 77 or 98%, respectively, although with an increase in completion time. (**E**) When assessed offline, the pattern recognition approach could discriminate up to 16 classes with accuracies greater than 94% for all movements and equal to 77.5% for resting. Misclassifications consisted mainly in individual finger movements recognized as resting. Actual classes (from up to down): palmar, lateral, and precision grasp; hand opening; wrist flexion and extension; wrist pronation and supination; radial and ulnar deviation; index and thumb flexion; thumb opposition; middle and little finger flexion; and resting.

(SVMs) with a one-versus-all approach and a majority voting post-processor (three of five classifications). This pattern recognition algorithm was a viable alternative to direct control given that different voluntary contraction patterns (wrist pronation, supination, and rest) resulted in linearly separable clusters in terms of distances and relative orientations between magnet pairs. However, although this separation was stable within a single fitting/donning of the prosthesis (intracluster radii, <0.5 mm; intercluster distances >1 mm), it was not across multiple donnings (Fig. 3C). Hence, it was necessary to retrain the model after each new donning of the prosthesis.

The SVM trained with three classes (radial deviation, supination, and resting) and was assessed in real time via a virtual test [similar to a motion test (*27*)] while the participant wore the prosthesis with the arm in a fixed position or with the arm reaching six different target positions (fig. S2), yielding completion rates of 100% and maximum completion times of 1.25 and 3 s, respectively (blue and green curves in Fig. 3D). The same virtual test was repeated by training the SVM with two sets of five classes—radial deviation, supination, middle finger extension, ulnar deviation, and resting—and the previous set with hand closing in place of middle finger extension. These two models were assessed while reaching six target positions and yielded completion rates of 77 or 98%, respectively, and maximum completion times of 4.05 or 6.35 s (red and yellow curves in Fig. 3D). Because such maximum completion times included the time to reach the target position, and (by definition) the 1-s hold period, these outcomes suggest that in most of the cases (~70%), the patient executed the trial and reacted to eventual misclassifications very quickly (less than 300 ms of overhead time).

The pattern recognition approach was also capable of discriminating up to 16 classes offline (including grasps, independent digit flexion, and wrist movements) with the arm in a single position, with accuracies greater than 94% for all movements and equal to 77.5% for the resting class (Fig. 3E). Errors mainly stemmed from the misclassification of classes corresponding to independent digit flexion movements as the resting class and vice versa.

Functional outcomes

The participant was able to complete functional tests commonly used to assess the dexterity of upper limb prostheses with both direct (MAG-DC) and pattern recognition (MAG-PR) controllers, using the implanted magnets (Fig. 4A and table S1). The myoelectric hand fitted before the surgery was also used to complete the functional tests for comparison (EMG-DC). In the Southampton Hand Assessment Procedure (SHAP), the participant achieved an index of function of 38 with the MAG-DC and of 52 with both the MAG-PR and the EMG-DC controller (MAG-DC in movie S1). The Minnesota Manual Dexterity Test (MMDT; placing only, three repetitions) yielded completion times of 807 s for the MAG-DC, 747 s for the MAG-PR, and 531 s for the EMG-DC controller. The clothespin relocation task (CRT) was completed in 52.84 s with the MAG-DC, 48.65 s with the MAG-PR, and 40.46 s with the EMG-DC controller, considering a cumulative completion time for upward and downward trials (MAG-PR in movie S2). The bimanual activity test (BAT), administered by a physiotherapist, showed that the limb fitted with the prosthesis under MAG-PR and EMG-DC control was equally integrated into bimanual activities (Fig. 4B). The pick and lift test (PLT) revealed improved motor coordination when using the MAG-PR compared with that when using the EMG-DC or MAG-DC controller. This outcome is corroborated by significantly lower ($P < 0.001$) temporal delays achieved with the MAG-PR compared with the other controllers, indicating the time interval in which the grip force reached 50% of the load force, and by a smoother increase in the grip force (Fig. 4C and fig. S4). According to the NASA Task Load Index (NASA TLX) questionnaire, the three controllers demanded similar (and generally low) physical and mental workloads (Fig. 4D).

Last, and anecdotally, the participant was able to perform a broad range of activities of daily living requiring fine movements, like manipulating fragile objects (an egg and a plastic glass) while moving the limb in space, extracting pills from a blister pack, or tying their shoes, with both DC and PR (EMG-DC and MAG-PR in movie S3 and MAG-PR in movie S4).

DISCUSSION

This study presents the clinical implementation of a self-contained myokinetic hand prosthesis controlled in real time in a transradial amputee. Implanted magnets and a transcutaneous magnetic localizer embedded in the prosthetic socket allowed for wireless, safe, and stable monitoring of muscle contractions over a 6-week study, clinically demonstrating the viability of this approach for the control of bionic hands. The closest study is that by Moradi *et al.* (*28*), who recently reported on the implantation of single magnets in three flexor forearm muscles of a transradial amputee in conjunction with a tendon transfer technique to increase magnet movement range and independence. The authors could demonstrate the clinical viability of the approach, albeit presenting only bench tests and mostly offline outcomes. Taylor *et al.* (*29*) also contributed to this idea by implanting pairs of magnets in a turkey animal model and demonstrating that multimagnet localization is more precise in close proximity to magnetic field sensors, even more than fluoromicrometry.

Although the minimal invasiveness of the implantation procedure led to a short surgery and recovery time, it also led to suboptimal placement of the magnets. Ultrasound examination showed that the implants were located just below the muscle fascia and not in the muscle belly. Thus, even if a displacement of more than 5 mm was observed preoperatively in all target muscles, only FPL_d had enough independence and an SNR high enough to implement direct control (fig. S1). Nevertheless, given that it was possible to decode motor intentions from the displacement of the magnets also using direct control, we demonstrated that myokinetic control can be modeled, with no need to resort to nonexplainable approaches, and that this solution is stable (fig. S1). Given this, it stands to reason that the availability of multiple independent control channels could allow parallel control over multiple movements, as the outcomes of the motion test and offline classifier suggest (Fig. 3, D and E), although this possibility could not be investigated in the present study. Restricted magnet displacement and elbow-related noise limited accurate recognition to only three classes during functional tests, preventing full exploitation of the dexterity of the robotic hand. In addition, for all controllers, the grasp type was predetermined by the experimenter, and thus the participant could not switch grasps during functional test execution. Nonetheless, the successful performance in functional tests with results not dissimilar to those of myoelectric controllers, a standard-of-care solution, suggests that the system is readily learnable, that is, intuitive, supporting the assumptions made in conceiving the myokinetic interface, the achievement of physiological control (*14*).

The technicalities associated with the mechanical disturbances did not result from the displacement of the socket relative to the skin, as expected (*21*), but from the movement of the elbow. Although not explicitly anticipated, the observed tissue displacements, on the order of a few millimeters, did not appear unexpected in retrospect, considering the elastic properties of muscle tissues (Fig. 1D). Contrary to what one would expect, elbow movements had a similar effect on the magnet pairs independently from the origin of the muscles (humerus for the FCU and radius for the FPL). This suggests that other factors, such as neighbor muscle deformations or socket-induced loadings, had a primary role in movement-related artifacts, which, however, were largely mitigated by the application of

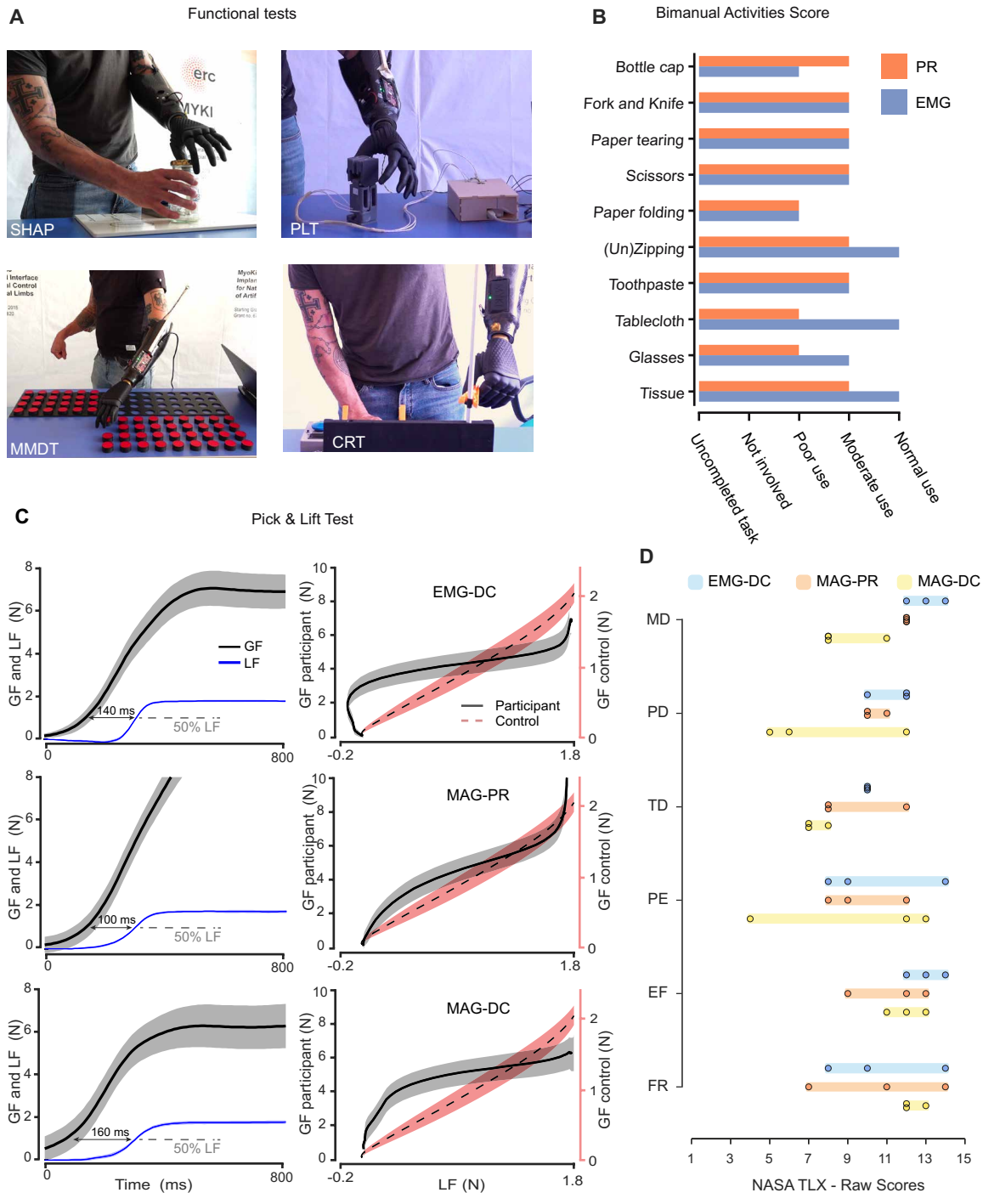

Fig. 4. Functional tests and physical and mental workload assessment. (**A**) Representative pictures of the participant carrying out the SHAP, PLT, MMDT, and CRT. (**B**) Scores of the BAT, performed with the EMG and the pattern recognition (PR) controllers. The obtained scores were similar and showed that in most cases, the impaired limb was moderately engaged in bimanual activities, which included unscrewing and screwing the cap of a water bottle; slicing a soft object using a fork and a knife; tearing a sheet of paper; cutting a sheet of paper in two with scissors; folding a sheet of paper and putting it in an envelope; opening and closing the zip of a pencil case; squeezing toothpaste onto a toothbrush; laying a tablecloth on a table; opening a case and taking out a pair of glasses; and opening a tissue package and taking out one tissue. (**C**) Motor coordination during the PLT for the EMG-DC, the MAG-DC, and the MAG-PR. The first column depicts the grip force (GF) and load force (LF) over time and the temporal delay. The second column compares the GF and LF profiles of the participant with those of a nonamputated individual (control condition). (**D**) Raw scores of the NASA TLX questionnaire (MD, PD, and TD are mental, physical, and temporal demand, respectively; PE, performance; EF, effort; FR, frustration) for all three controllers showed that the latter demanded similar (and generally low) physical and mental workload to complete functional tasks. The three dots refer to the scores assigned by the participant after performing the SHAP, CRT, and PLT. The MMDT and BAT scores were not reported because they were not acquired for all controller types.

differential measurements in the FPL and FCU, achieving disturbances below 2 mm (Fig. 1D). This result implies that movement artifacts could be neglected by implementing rejection strategies akin to differential measurements in case an enhanced surgical insertion of the magnets enables larger contraction shifts because of voluntary activations. However, because elbow-induced displacement was of the same order of magnitude as that caused by voluntary contraction in this case, it posed a problem for direct control that was solved through the enable/disable switch based on the elbow speed. Differently, the ED muscle, especially in its proximal segment, was severely affected by the physical folding of the socket during elbow flexion, which amplified the mechanical disturbance on the implanted magnets up to 25 mm. The 6 weeks available for the study, combined with the number of planned tests, did not allow us to manufacture a better socket; hence, we had to drop ED_p and ED_d as potential control signals. This inconvenience suggested that in future studies, the implant sites should also be identified by considering socket constraints or that the socket design should be revised to reduce the system footprint, as discussed in the following paragraph.

We hypothesized the need to retrain the pattern recognition model to be partly caused by a variable/unpredictable deformation induced by the socket on the soft tissues in multiple donnings, affecting the input feature space. In addition to that, different donnings, as well as arm swelling due to day-long usage, likely caused millimetric changes in sensor placement relative to the implanted magnets, which possibly led to a different convergence point of the localization algorithm. Similarly, a slight sensor-to-magnet shift occurred during intradonning acquisitions after repeated elbow movements. This led to minor socket movements and the formation of intraclass-shifted data clusters, although the classes remained separable (Fig. 1C). Further investigation of these factors should lead to strategies to improve the robustness and generalization of the control algorithms.

Results obtained with the PLT, especially with the MAG-PR, suggested a good integration of the prosthesis in the sensorimotor control loop of the participant, although the control on the grip force was poor, because this force did not reach a plateau after object lifting (Fig. 4C). Yet, the improved motor coordination achieved with the MAG-PR compared with the EMG-DC controller was demonstrated by a temporal delay approaching that of participants without physical impairment and an approximately constant ratio between grip and load force (*30*) (Fig. 4C). The MAG-DC controller was perceived as slower and less responsive compared with the MAG-PR because of the elbow-controlled switch, as evidenced by a higher temporal delay (Fig. 4C). As mentioned above, we propose that substantial improvement to this issue could be achieved by implanting the magnets in muscle sites enabling higher displacement, in other words, higher SNR. Yet, the higher motor coordination achieved by the MAG-PR suggests that there is large room for improvement, especially considering the limited timeframe of this study. In this context, conveying relevant sensory feedback through physiological channels would potentially refine dexterity and support the integration of the artificial limb in performing functional tasks. Notably, by triggering remote vibrations in the magnets using an external stimulator, we could potentially activate proprioceptive muscle receptors or mechanoreceptors in the muscles or skin, thus eliciting natural kinesthetic and vibrotactile sensations. If these strategies are effective, the myokinetic interface would be able to provide the user with bidirectional direct communication with the prosthesis, like the natural hand. The use of untethered vibrations to elicit intracorporeal sensations was investigated during this study using a bench device developed and characterized in previous studies (*15*), and the outcomes of feedback experiments are being investigated in a separate study.

This clinical implementation provided important guidelines for future studies, including a better understanding of the actual pros and cons brought by this approach. First, there are key aspects to consider in the recruitment process: Optimal candidates should have a recent amputation, trained and nonatrophied muscles, no fibrosis or denervated areas, and a relatively long stump. These are all factors that allow for larger displacement of residual muscles and thus contribute to increasing the SNR for control. Although they appear to be restrictive inclusion criteria, many new surgical techniques are becoming available for residual limb treatment that may improve muscle mobility and access to independent muscle patterns. Among these, we cite targeted muscle reinnervation (TMR), which creates novel control sources by grafting severed nerves from the stump into surrogate muscles (*31*). We already suggested the opportunity to merge TMR with the myokinetic interface (*32*), and hence, reinnervated muscles exhibit a large displacement during contraction and distinguishable activation patterns after different movements. Combination with different surgeries readily translates into combination with other amputation levels, for example, glenohumeral amputations with TMR or transtibial amputations treated with the agonist-antagonist myoneural interface (*33*), that could be achieved by embedding the system electronics in the chest and leg suspension system, respectively. Furthermore, a proper redesign of the hardware of the TML, such as reduced dimensions of the sensor boards to match the socket curvature, would allow for reduction of the system footprint, which could be housed in a less bulky and more flexible enclosure around the stump. If combined with advanced suspension systems like osseointegration (*9*, *10*), exploiting nonferromagnetic implants, this solution would substantially improve user comfort, thus addressing a major factor contributing to prosthetic abandonment (*34*). In this case, the system electronics could be housed in smaller and lighter frames (such as bracelets) to be worn around the residual limb. Last, the transition to chronic implants will require the development of coating solutions for the magnets that provide adequate robustness and durability.

Synthetizing all these factors and assuming improved placement of the magnets inside the muscles, the myokinetic interface holds the potential to reveal unique signals related to specific phantom limb movements, allowing achievement of natural and sophisticated control strategies. Although alternative noninvasive solutions like sonomyography (*35*, *36*) have been proposed for the monitoring of muscle displacement, the myokinetic interface holds the potential to enable a higher level of selectivity and functionality, akin to the enhanced performance demonstrated by implantable electrodes with respect to surface ones in EMG control (*9*). A comparison between the performance of the myokinetic interface and that of commercially available pattern recognition controllers remains to be assessed. For example, single muscle movements could be used to control the speed of corresponding movements in the robotic hand; for instance, the displacement measured in the thumb flexor could proportionally drive the flexion of the robotic thumb. Complementing this, the delivery of feedback through remote vibration would allow the user to provide relevant sensory feedback which, albeit non-somatotopically matched and not entirely natural, would allow

the user to build an internal model of the motor task and because of this to grasp in a predictive feedforward fashion. To conclude, the results achieved in such a short period of time suggested the potential of the myokinetic interface to restore long-sought natural motor control in people who have lost their limbs.

MATERIALS AND METHODS

Study design

All surgical and experimental procedures were carried out at AOUP (Azienda Ospedaliero Universitaria Pisana) Hospital. The study protocols were carried out in accordance with the Declaration of Helsinki. The study was approved by the Ethical Committee of AOUP and the national competent authorities. Before obtaining a signed informed consent, the participant was informed about the nature and possible consequences of the study, and eligibility was checked against the study inclusion/exclusion criteria. Consent to publish identifiable images of research participants was obtained from the participant and notified to the competent authorities.

The participant then underwent preoperative clinical evaluations to assess the functionality of the residual muscles in terms of contraction capabilities and eventual presence of fibrotic tissue or muscle atrophy. Nine residual muscles were preliminary evaluated, namely, pronator, flexor carpi radialis, FCU, flexor digitorum superficialis, flexor digitorum profundus, extensor carpi radialis, ED, brachioradialis, and FPL. All of them were eligible for implant, and consequently, target muscles were selected on the basis of the complementarity of their functions: a flexor muscle (FCU), an extensor muscle (ED), and a muscle actuating the thumb (FPL).

For comparison with standard-of-care solutions, the week before the implantation, we fitted the participant with a two-state amplitude modulated myoelectric controller. To this aim, a custom resin self-suspending socket was fabricated. It included stainless steel electrodes (Ottobock Inc.) placed above the flexor and extensor muscles of the wrist, providing the closing and opening of the hand, respectively. The participant was administered state-of-the-art tests commonly used to assess the functionality of upper limb prostheses, namely, the SHAP, in which the participant grasps a variety of objects (*37*); the MMDT, in which the participant places a series of cylinders in matched holes (*38*); the CRT, where the participant moves three clothespins from a horizontal to a vertical pole (*39*); the BAT, administered by a physiotherapist, which assesses the degree of integration of the impaired limb in bimanual tasks (*40*). In addition, the participant performed the PLT, a well-established procedure in motor control studies (*41*) used to assess the integration of sensorimotor control paradigms. The NASA TLX was administered at completion of the functional tests to evaluate the physical and mental workload (*42*). The McGill Pain Questionnaire was also administered to provide a quantitative measure of pain related to the phantom limb before surgery (*25*). Furthermore, we recorded videos of the participant performing activities of daily living (ADLs), including unscrewing a jar/bottle cap, manipulating a fragile object (plastic glass), extracting pills from a blister pack, slicing a soft object with a knife, holding a rubber ball or an egg while moving the arm in space, and tying shoes. These videos allowed us to qualitatively assess (i) the robustness of the controller against the limb movements in space and (ii) the ability of the participant to finely control the prosthesis.

The participant subsequently underwent the implantation surgery, followed by a 1-week rest period that allowed the surgical wounds to heal. During the following 5 weeks, experimental sessions to implement and assess the myokinetic control interface were carried out at AOUP 3 days a week. Ultrasound imaging was used to monitor magnet position and displacement caused by muscle contraction throughout the whole implantation period. Specifically, an ultrasound scanner (MyLab Omega, Esaote s.p.a.) was used to acquire videos of the FCU, ED, and FPL muscles, in both the longitudinal and the transverse muscle planes, while the participant was performing nonfatiguing movements corresponding to a prevalent activation of each of the three implanted muscles, i.e., ulnar deviation, four-digit extension, and thumb flexion, respectively. These videos were analyzed offline to retrieve the displacement undergone by each magnet with respect to its position at rest (relaxed muscle state). Regarding the implementation of the control strategy, the first 2 weeks were dedicated to prosthetic fitting and to the characterization of the candidate control inputs and potential sources of disturbance. On the basis of the outcomes of this characterization, the last 3 weeks were dedicated to the implementation of two different myokinetic controllers (direct and pattern recognition–based, see below). The evolution of the pain associated with the phantom limb throughout the implantation period was monitored by administering the McGill Pain Questionnaire on a weekly basis.

TML

The TML used in the study and its performance in terms of computation time, power consumption, and localization precision/accuracy were comprehensively described in our recent work (*24*). Briefly, the system included seven acquisition units (AUs), each hosting 20 magnetic field sensors, one geomagnetic field compensation sensor, and a microprocessor-based computation unit (CU), based on the i.MX RT1060 real-time processor running on an Arm Cortex-M7 core at 600 MHz. The AUs were arranged above the implanted muscles in locations empirically selected to ensure accurate and stable localizations. The AUs sampled synchronously, meaning that readings from the 140 sensors occurred all at the same time instant, thus ensuring consistent measurements. After sampling, the AUs sequentially transferred the acquisitions to the CU, which retrieved the poses of the magnets by feeding them to the localization algorithm, operating in pipeline (concurrently) with the AU sampling and AU-CU data transferring. The AU-CU rates, defined as the interval of time at which complete data packages were transmitted to the CU, were equal to ~23.6 ms, which coincided with the output rate of the whole system, unless the localization algorithm took more time.

Akin to our previous works, the CU derived the poses of the six magnets by modelling the field at the ith sensor as a linear superposition of that produced by six magnetic dipoles and reversing these equations through numerical approximation methods. Specifically, the CU ran the Levenberg-Marquardt algorithm (LMA) for each new data package received from the AUs and considered the results acceptable only if the magnets were localized within a user-defined workspace. Such a workspace (or volume) was set at the first donning of the prosthesis through a calibration procedure lasting a few minutes, in which the participant was asked to contract the implanted muscles while moving the limb in space, e.g., bending the elbow and shoulder. After obtaining a comprehensive set of localizations, the final volumes were determined by adding a 2-cm safety bias to the minimum and maximum x, y, and z coordinates at which each magnet was localized. These volumes were subsequently stored in

the nonvolatile memory of the CU and used at following donnings. A light-emitting diode on the CU blinked green during normal use but turned violet when a magnet was retrieved outside of its volume, in which case the localization was marked as incorrect and the LMA was rerun until a correct localization was achieved. The violet blinking informed the user and experimenters of incorrect functioning and the possible need to repeat the calibration.

Prosthetic fitting

After the rest week postsurgery, the participant was fitted with a custom-made temporary self-suspending resin socket that allowed free placement of a variable number of AUs on its external surface. As mentioned above, we empirically searched for an AU number and placement that ensured a stable localization of the six implanted magnets and found optimal localization precision (repeatability) using seven AUs placed above the implantation sites. The AU selection was achieved by exploiting a custom graphical interface coded through the processing graphical library, which displayed in real time the current poses of the magnets and the AUs and allowed us to save localization and acquisition data for further offline analysis. The socket could not be connected to the prosthesis, and thus it was used during the first two experimental weeks to characterize the available control signals (see below) while the final socket was being manufactured by a prosthetist. The latter was a custom-made carbon fiber self-suspending socket that integrated all TML components in dedicated slots. Specifically, it included slots to host the seven AUs in the optimal selected locations and two additional pockets on the outer layer and accessible from the outside that hosted the CU and the battery used to power both the TML and the robotic hand. In addition, the geomagnetic field compensation sensor was mounted on a nonferromagnetic stick attached on the outside of the prosthetic socket, away from the implanted magnets (Fig. 4A).

Signal characterization

Different datasets were acquired to investigate the candidate signals for control and the type and extent of potential disturbances. For this purpose, we developed a custom graphical user interface (GUI) using C# in Visual Studio (Microsoft Corporation) to instruct the participant to perform specific movements while acquiring synchronized localization data from the TML.

To evaluate the independence of the three myokinetic channels at different limb positions, the GUI showed sequences of steps that the participant had to match by contracting the implanted muscles while performing different movements. Specifically, the participant was asked to perform different movements expected to induce a prevalent activation in ED, FCU, and FPL with both an extended and flexed elbow. These movements were, respectively, four-digit extension and wrist extension for ED, ulnar deviation and wrist supination for FCU, and radial deviation and wrist pronation for FPL (after excluding thumb flexion because the induced contraction shift with the prosthesis on was poor). To avoid muscle fatiguing, contractions were divided into steps of 3 s, separated by relaxation intervals of 8 s. The acquisitions were repeated multiple times during the implantation period to assess the stability of the contractions over the weeks and the intra- and interday variability due to multiple donnings of the prosthesis or arm swelling (fig. S1). The same acquisition protocol was also sporadically used to assess muscle activation induced by other common grasps (such as palmar, precision, and lateral grasp), flexion/extension of the individual fingers, and ab-adduction of the thumb. The GUI temporized the activation and rest intervals and provided real-time feedback by displaying the contraction shift of three user-defined magnet pairs over the step sequences. At the end of each acquisition, localization data were saved in a text file for offline analysis.

To investigate the effect of limb movements on the distance at rest between magnet pairs and disentangle it from voluntary muscle activation, we asked the participant to move the elbow and shoulder following sinusoidal waves with different periods (8, 6, 4, 3, and 2 s) displayed on the GUI while keeping the implanted muscles relaxed. In particular, the participant performed elbow medial/lateral rotation and elbow and shoulder flexion/extension, and the mapping between joint angle and localization data was obtained by concurrently tracking optical markers arranged on the wrist, elbow, and shoulder of the impaired limb through a three-camera six-DoF optical tracking system (V120:Trio, OptiTrack, US) (fig. S3). Moreover, to evaluate the feasibility of modulating muscle activation and capturing such modulation through localization, we asked the participant to mirror the same sinusoidal waves by gradually contracting the implanted muscles. This exercise was performed only for the movements that had demonstrated sufficient SNR and robustness against limb movements in the sequence of steps.

This signal characterization procedure led to the identification of the optimal strategy and signals to implement the direct controller. In addition, the same GUI was also used to acquire the data for training the pattern recognition controller, as described below.

Direct control

After signal characterization, the contraction shift between FPL_d and FCU_d induced by wrist pronation and supination was identified as the optimal signal to control the closing and opening of the robotic hand, respectively. In addition, the speed of the contraction shift between the magnets in ED was used to counteract the artifacts caused by limb movements, in particular by elbow flexion/extension. According to this, the controller was implemented as a four-state machine in which the robotic hand could be in the following states: disabled state, i.e., no control input could be sent to the hand when the slope related to the magnets in ED overcame a set threshold, th3; opening state, when the contraction shift caused by supination overcame a set threshold, th2; closing state, when the contraction shift caused by pronation overcame a set threshold, th1; rest state, when none of the previous thresholds was overcome. The value of the distance at rest between FPL_d and FCU_d was updated to take into account slow variations caused by different factors over time (such as slow limb movements). Practically, two moving average filters with a 90-ms and a 1-s window were applied at discrete steps of 50 ms, in accordance with the robotic hand control frequency, to update the current and magnet distance at rest, respectively. The difference between these two measures, i.e., the contraction shift between FPL_d and FCU_d, was subsequently compared against the set thresholds th2 and th3. In addition, proportional speed control was implemented by linearly mapping the retrieved contraction shift to the opening and closing speed of the hand. The GUI was used to tune the value of th1, th2, and th3 and to transmit the updated values to the CU, which implemented the control algorithm and sent the appropriate command to the hand, i.e., the degree of opening/closing in the current grasp type (palmar, precision, or lateral).

The direct controller was assessed quantitatively by administering the same functional test used to evaluate the EMG controller

(except the BAT) and qualitatively by repeating the same ADLs. Accordingly, the NASA TLX was used to evaluate the physical and mental workload required to complete each functional test. Because of the limited timeframe of the study and the time needed to characterize the signals/develop the final prosthetic socket, functional tests were repeated only once for each controller type (i.e., MAG-DR and MAG-PR, see below) during the last two implantation weeks. For this reason, performance achieved with different controllers (including EMG-DR) could not be statistically compared, except for PLT, which involved 100 repetitions of the lifting task. A nonparametric multicomparison test was applied to compare the temporal delays achieved using the different controllers across all repetitions. Specifically, because data were found to be nonnormally distributed according to the Kolmogorov-Smirnov test, the Kruskal-Wallis test with Bonferroni correction was applied.

Pattern recognition

We used an SVM classifier with a linear kernel to map the coactivity pattern of a muscle group associated with a virtual movement of the phantom limb to a corresponding movement of the robotic hand. More specifically, multiple classifiers were trained to selectively recognize an equal number of classes, and a one-versus-all approach was applied at the training stage to determine the class with the highest score. At testing time, the latter was determined on the basis of a majority voting approach, according to which the class that obtained the highest score in at least three of five previous iterations was ultimately selected as the winner. The same GUI was used to acquire the data for training the models, which consisted of a number of individually acquired movements alternating 5 s of muscle contraction with 5 s of muscle relaxation (rest). To increase the robustness of the classifier, the movements were acquired while the participant kept the limb in different positions, including elbow extended on the side, elbow flexed at 90°, reaching forward (i.e., as to pick up an object on the table), and shoulder flexed at 135° (as to grasp an object placed on top). To train the model, the participant was required to perform three repetitions of each movement in each limb position, resulting in a retraining time of <2 min per movement, akin to similar myoelectric controllers (*43*–*45*). The GUI temporized the contraction and relaxation phases and saved the output of the localization in a text file.

Subsequent offline analysis was implemented to extract 30 time series describing the linear and angular distances between all possible magnet pairs (15 in total, one linear and one angular for each pair). The angular distance was computed as the 3D angle between the magnetization vectors of each magnet pair. Because of a limitation of the CU hardware resources, 18 (nine linear and nine angular distances) of the 30 series, corresponding to nine magnet pairs that showed observable patterns associated with muscle activation, were empirically selected for model training and testing. To ensure that training was performed on the steady portion of the signal, the central 2.5 s of the contraction and rest intervals of each selected time series were extracted and concatenated. The feature set was ultimately obtained by normalizing the median value of the samples contained in windows of 200 ms, with a 150-ms overlap. These features were used to train the classifiers on Matlab 2017b (MathWorks Inc.) and subsequently derive the SVM parameters to be transmitted to the CU that implemented the embedded classifier. During real-time operation, the latter provided new predictions every 50 ms.

We tested the real-time performance of the classifier by implementing a three-class model able to discriminate hand opening (trained on wrist supination data), hand closing (trained on wrist pronation or radial deviation data), and resting. The trained classifier was used to control the robotic hand and perform the same functional tests (including the BAT) and ADLs carried out with the EMG controller and the myokinetic direct controller, including the NASA TLX at test completion. In addition, the real-time performance of the classifier was assessed with a modified motion test carried out in two different configurations: with the participant sitting and resting the arm on a support and with the participant standing and performing different movements in six different arm positions. The training dataset acquired in the first configuration included three repetitions of two movements, radial deviation and wrist supination. The training dataset acquired in the second configuration included three repetitions of six movements: radial deviation, wrist supination, wrist extension, ulnar deviation, middle finger extension, and hand closing. The latter movements were repeated holding the arm in six different positions, namely, shoulder flexed at 45°, 90°, and 135°; elbow flexed at 90%; and reaching forward obliquely to the left and to the right (fig. S2). Different combinations of the movements acquired in the second configuration were used to train three classifiers, including the following classes: radial deviation and supination; the previous as well as middle finger extension and ulnar deviation; the previous with hand closing in place of middle finger extension. According to this, the test evaluated the feasibility of discriminating in real time a maximum of five classes. During the test, the participant was asked to wear the robotic hand to reproduce realistic loading conditions on the stump. In line with previous studies from the literature (*27*, *45*), the motion test required 20 correct predictions within 10 s to consider a motion completed. Standard metrics were used to evaluate the test outcomes, namely, the completion time, consisting of the time between the first prediction different from resting and the 20th correct prediction, and the completion rate, consisting of the number of completed motions over the total number of motions attempted. Specifically, for each trial and its corresponding completion time, we calculated the completion rate as the number of completed motions within that trial time relative to the total attempted motions. The deviation from the standard test was that, unlike what is generally reported in the literature, the completion time also included the time to reach the target position from rest (that is, with the arm extended to the side).

Last, a larger dataset comprising up to 15 movements (plus rest), including grasps, wrist movements, single finger flexion/extension, and thumb adduction/abduction, was acquired in the third week after implantation to assess offline the feasibility of discriminating many classes. The participant, while seating with the socket steady on the armchair, repeated each movement 15 times (5-s contraction and 5-s rest). Accuracy was evaluated using a fivefold cross-validation procedure involving 12 repetitions per movement for training and three for testing. Resting data were uniformly down-sampled across the entire dataset to achieve class balance.

Statistical analysis

The acquired data were exported and processed offline in MATLAB 2017b (MathWorks). All data are reported as mean values ± SD (unless elsewise indicated). The normality of data distributions was verified. In cases of non-Gaussian distribution, we performed two-tailed Kruskal-Wallis tests. Post hoc correction was executed in cases

of multiple groups of data. The significance level was 0.05. In the captions of the figures, we report the used statistical tests/measure for each analysis and its result, along with the numerosity of the distributions/the number of repetitions. Last, Pearson and Spearman coefficients were computed to assess the presence of increasing/decreasing linear or monotonic trends resulting from voluntary contractions and elbow flexion/extension on magnet displacement, considering multiple acquisitions repeated throughout the implantation period.

Supplementary Materials

The PDF file includes:
Figs. S1 to S4
Table S1

Other Supplementary Material for this manuscript includes the following:
Movies S1 to S4

REFERENCES AND NOTES

1. E. Scheme, K. Englehart, Electromyogram pattern recognition for control of powered upper-limb prostheses: State of the art and challenges for clinical use. *J. Rehabil. Res. Dev.* **48**, 643 (2011).
2. A. D. Roche, H. Rehbaum, D. Farina, O. C. Aszmann, Prosthetic myoelectric control strategies: A clinical perspective. *Curr. Surg. Rep.* **2**, 44 (2014).
3. D. Farina, I. Vujaklija, R. Brånemark, A. M. J. Bull, H. Dietl, B. Graimann, L. J. Hargrove, K. P. Hoffmann, H. Huang, T. Ingvarsson, H. B. Janusson, K. Kristjánsson, T. Kuiken, S. Micera, T. Stieglitz, A. Sturma, D. Tyler, R. F. ff Weir, O. C. Aszmann, Toward higher-performance bionic limbs for wider clinical use. *Nat. Biomed. Eng.* **7**, 473–485 (2021).
4. A. D. Roche, Z. K. Bailey, M. Gonzalez, P. P. Vu, C. A. Chestek, D. H. Gates, S. W. P. Kemp, P. S. Cederna, M. Ortiz-Catalan, O. C. Aszmann, Upper limb prostheses: Bridging the sensory gap. *J. Hand Surg. Eur. Vol.* **48**, 182–190 (2023).
5. S. Raspopovic, M. Capogrosso, F. Petrini, M. Bonizzato, J. Rigosa, G. Di Pino, J. Carpaneto, S. Micera, Restoring natural sensory feedback in real-time bidirectional hand prostheses. *Sci. Transl. Med.* **6**, 222ra19 (2014).
6. D. W. Tan, M. A. Schiefer, M. W. Keith, J. R. Anderson, J. Tyler, D. J. Tyler, A neural interface provides long-term stable natural touch perception. *Sci. Transl. Med.* **6**, 257ra138 (2014).
7. J. A. George, D. M. Page, T. S. Davis, C. C. Duncan, D. T. Hutchinson, L. W. Rieth, G. A. Clark, Long-term performance of Utah slanted electrode arrays and intramuscular electromyographic leads implanted chronically in human arm nerves and muscles. *J. Neural Eng.* **17**, 056042 (2020).
8. S. Raspopovic, G. Valle, F. M. Petrini, Sensory feedback for limb prostheses in amputees. *Nat. Mater.* **20**, 925–939 (2021).
9. M. Ortiz-Catalan, B. Håkansson, R. Brånemark, An osseointegrated human-machine gateway for long-term sensory feedback and motor control of artificial limbs. *Sci. Transl. Med.* **6**, 257re6 (2014).
10. M. Ortiz-Catalan, J. Zbinden, J. Millenaar, D. D'Accolti, M. Controzzi, F. Clemente, L. Cappello, E. J. Earley, E. Mastinu, J. Kolankowska, M. Munoz-Novoa, S. Jönsson, C. Cipriani, P. Sassu, R. Brånemark, A highly integrated bionic hand with neural control and feedback for use in daily life. *Sci. Robot.* **8**, eadf7360 (2023).
11. P. F. Pasquina, M. Evangelista, A. J. Carvalho, J. Lockhart, S. Griffin, G. Nanos, P. McKay, M. Hansen, D. Ipsen, J. Vandersea, J. Butkus, M. Miller, I. Murphy, D. Hankin, First-in-man demonstration of a fully implanted myoelectric sensors system to control an advanced electromechanical prosthetic hand. *J. Neurosci. Methods* **244**, 85–93 (2015).
12. P. P. Vu, A. K. Vaskov, Z. T. Irwin, P. T. Henning, D. R. Lueders, A. T. Laidlaw, A. J. Davis, C. S. Nu, D. H. Gates, R. B. Gillespie, S. W. P. Kemp, T. A. Kung, C. A. Chestek, P. S. Cederna, A regenerative peripheral nerve interface allows real-time control of an artificial hand in upper limb amputees. *Sci. Transl. Med.* **12**, eaay2857 (2020).
13. MYKI ERC Project; http://www.mykierc.eu/.
14. S. Tarantino, F. Clemente, D. Barone, M. Controzzi, C. Cipriani, The myokinetic control interface: Tracking implanted magnets as a means for prosthetic control. *Sci. Rep.* **7**, 17149 (2017).
15. J. Montero, F. Clemente, C. Cipriani, Feasibility of generating 90 Hz vibrations in remote implanted magnets. *Sci. Rep.* **11**, 15456 (2021).
16. R. Merletti, P. Parker, *Electromyography: Physiology, Engineering, and Non-Invasive Applications* (Wiley, 2004).
17. G. Yamaguchi, *Dynamic Modeling of Musculoskeletal Motion: A Vectorized Approach For Biomechanical Analysis In Three Dimensions* (Springer, 2005).
18. J. A. Hoffer, G. E. Loeb, Implantable electrical and mechanical interfaces with nerve and muscle. *Ann. Biomed. Eng.* **8**, 351–360 (1980).
19. M. Gherardini, F. Clemente, S. Milici, C. Cipriani, Localization accuracy of multiple magnets in a myokinetic control interface. *Sci. Rep.* **11**, 4850 (2021).
20. F. Masiero, E. Sinibaldi, F. Clemente, C. Cipriani, Effects of sensor resolution and localization rate on the performance of a myokinetic control interface. *IEEE Sens. J.* **21**, 22603–22611 (2021).
21. F. Paggetti, M. Gherardini, A. Lucantonio, C. Cipriani, To what extent implanting single vs pairs of magnets per muscle affect the localization accuracy of the myokinetic control interface? Evidence from a simulated environment. *IEEE Trans. Biomed. Eng.* **70**, 2972–2979 (2023).
22. S. Milici, M. Gherardini, F. Clemente, F. Masiero, P. Sassu, C. Cipriani, The myokinetic control interface: How many magnets can be implanted in an amputated forearm? Evidence from a simulated environment. *IEEE Trans. Neural Syst. Rehabil. Eng.* **28**, 2451–2458 (2020).
23. F. Clemente, V. Ianniciello, M. Gherardini, C. Cipriani, Development of an embedded myokinetic prosthetic hand controller. *Sensors* **19**, 3137 (2019).
24. V. Ianniciello, M. Gherardini, C. Cipriani, Transcutaneous magnet localizer for a self-contained myokinetic prosthetic hand. *IEEE Trans. Biomed. Eng.* **71**, 1068–1075 (2024).
25. R. Melzack, S. N. Raja, The McGill Pain Questionnaire: From description to measurement. *Anesthesiology* **103**, 199–202 (2005).
26. L. J. Hargrove, L. A. Miller, K. Turner, T. A. Kuiken, Myoelectric pattern recognition outperforms direct control for transhumeral amputees with targeted muscle reinnervation: A randomized clinical trial. *Sci. Rep.* **7**, 13840 (2017).
27. T. Kuiken, G. Li, B. Lock, R. Lipschutz, L. A. Miller, K. A. Stubblefield, K. B. Englehart, Targeted muscle reinnervation for real-time myoelectric control of multifunction artificial arms. *JAMA* **301**, 619–628 (2009).
28. A. Moradi, H. Rafiei, M. Daliri, M.-R. Akbarzadeh-T, A. Akbarzadeh, A.-M. Naddaf-Sh., S. Naddaf-Sh., Clinical implementation of a bionic hand controlled with kineticomyographic signals. *Sci. Rep.* **12**, 14805 (2022).
29. C. R. Taylor, S. S. Srinivasan, S. H. Yeon, M. K. O. Donnell, T. J. Roberts, H. M. Herr, Magnetomicrometry. *Sci. Robot.* **6**, eabg0656 (2021).
30. R. S. Johansson, G. Westling, Roles of glabrous skin receptors and sensorimotor memory in automatic control of precision grip when lifting rougher or more slippery objects. *Exp. Brain Res.* **56**, 550–564 (1984).
31. T. A. Kuiken, L. A. Miller, R. D. Lipschutz, B. A. Lock, K. Stubblefield, P. D. Marasco, P. Zhou, G. A. Dumanian, Targeted reinnervation for enhanced prosthetic arm function in a woman with a proximal amputation: A case study. *Lancet* **369**, 371–380 (2007).
32. M. Gherardini, A. Sturma, A. Boesendorfer, V. Ianniciello, A. Mannini, O. C. Aszmann, C. Cipriani, Feasibility study on disentangling muscle movements in TMR patients through a myokinetic control interface for the control of artificial hands. *IEEE Robot. Autom. Lett.* **7**, 7240–7246 (2022).
33. S. S. Srinivasan, G. Tuckute, J. Zou, S. Gutierrez-Arango, H. Song, R. L. Barry, H. M. Herr, Agonist-antagonist myoneural interface amputation preserves proprioceptive sensorimotor neurophysiology in lower limbs. *Sci. Transl. Med.* **12**, eabc5926 (2020).
34. S. Salminger, H. Stino, L. H. Pichler, C. Gstoettner, A. Sturma, J. A. Mayer, M. Szivak, O. C. Aszmann, Current rates of prosthetic usage in upper-limb amputees–Have innovations had an impact on device acceptance? *Disabil. Rehabil.* **44**, 3708–3713 (2022).
35. Y. P. Zheng, M. M. F. Chan, J. Shi, X. Chen, Q. H. Huang, Sonomyography: Monitoring morphological changes of forearm muscles in actions with the feasibility for the control of powered prosthesis. *Med. Eng. Phys.* **28**, 405–415 (2006).
36. V. Nazari, Y. P. Zheng, Controlling upper limb prostheses using sonomyography (SMG): A review. *Sensors* **23**, 1885 (2023).
37. Southampton Hand Assessment Procedure; http://www.shap.ecs.soton.ac.uk/index.php.
38. J. Desrosiers, A. Rochette, R. Hébert, G. Bravo, The Minnesota Manual Dexterity Test: Reliability, validity and reference values studies with healthy elderly people. *Can. J. Occup. Ther.* **64**, 270–276 (1997).
39. T. A. Kuiken, G. A. Dumanian, R. D. Lipschutz, L. A. Miller, K. A. Stubblefield, The use of targeted muscle reinnervation for improved myoelectric prosthesis control in a bilateral shoulder disarticulation amputee. *Prosthet. Orthot. Int.* **28**, 245–253 (2004).
40. J. H. Lee, I. Hong, J. H. Park, J. H. Shin, Validation of Yonsei-Bilateral Activity Test (Y-BAT)-bilateral upper extremity inventory using Rasch analysis. *OTJR: Occup. Ther. J. Res.* **40**, 277–286 (2020).
41. R. S. Johansson, G. Westling, Coordinated isometric muscle commands adequately and erroneously programmed for the weight during lifting task with precision grip. *Exp. Brain Res.* **71**, 59–71 (1988).
42. S. G. Hart, "NASA Task Load Index (TLX)" (20000021487, NASA, 1986).
43. D. D'Accolti, K. Dejanovic, L. Cappello, E. Mastinu, M. Ortiz-Catalan, C. Cipriani, Decoding of multiple wrist and hand movements using a transient EMG classifier. *IEEE Trans. Neural Syst. Rehabil. Eng.* **31**, 208–217 (2023).
44. A. M. Simon, K. L. Turner, L. A. Miller, B. K. Potter, M. D. Beachler, G. A. Dumanian, T. A. Kuiken, User performance with a transradial multi-articulating hand prosthesis

during pattern recognition and direct control home use. *IEEE Trans. Neural Syst. Rehabil. Eng.* **31**, 271–281 (2022).
45. M. Ortiz-Catalan, B. Håkansson, R. Brånemark, Real-time and simultaneous control of artificial limbs based on pattern recognition algorithms. *IEEE Trans. Neural Syst. Rehabil. Eng.* **22**, 756–764 (2014).

Acknowledgments: We thank our participant for commitment and trust. **Funding:** This work was funded by the European Research Council under the MYKI Project in 2015 (ERC-2015-StG, grant no. 679820). This work was also supported by the Italian Ministry of Research, under the complementary actions to the NRRP "Fit4MedRob - Fit for Medical Robotics" grant (# PNC0000007). **Author contributions:** M.G., V.I., F.M., F.P., D.D., E.L.F., and K.D. performed experiments and analyzed data. N.F., L.M., S.D., and C. Chisari conducted the neurophysiological tests and supervised the administration of the BAT test. E.I., O.M., and L.A. carried out the implantation and explanation surgical procedures. M.N. managed anesthesia during surgical interventions. M.G. wrote the paper with V.I. and C. Cipriani, and all the authors contributed to its editing. C. Cipriani conceived and supervised the whole study. **Competing interests:** C. Cipriani and M.C. hold shares in Prensilia S.r.l. **Data and materials availability:** All data are available in the main text or the Supplementary Materials.

Submitted 20 March 2024
Accepted 15 August 2024
Published 11 September 2024
10.1126/scirobotics.adp3260

Post date 18 December 2024

Erratum for the Research Article "Restoration of grasping in an upper limb amputee using the myokinetic prosthesis with implanted magnets" by M. Gherardini *et al*.

In the Research Article "Restoration of grasping in an upper limb amputee using the myokinetic prosthesis with implanted magnets" by M. Gherardini *et al*., an error in Fig. 2 caused some visual elements in (A), including the red and blue parts of the cylinders and other parts of the prosthetic socket (such as the prosthetic's battery, in blue), to become obscured. The figure has been corrected, and the conclusions and other data in the paper are not affected.

Science Robotics

Restoration of grasping in an upper limb amputee using the myokinetic prosthesis with implanted magnets

Marta Gherardini, Valerio Ianniciello, Federico Masiero, Flavia Paggetti, Daniele D'Accolti, Eliana La Frazia, Olimpia Mani, Stefania Dalise, Katarina Dejanovic, Noemi Fragapane, Luca Maggiani, Edoardo Ipponi, Marco Controzzi, Manuela Nicastro, Carmelo Chisari, Lorenzo Andreani, and Christian Cipriani

Sci. Robot. **9** (94), eadp3260. DOI: 10.1126/scirobotics.adp3260

Editor's summary

Restoration of dexterous motor control after an amputation is challenging in the field of prosthetics and often relies on transduction of electrical signals from the brain to control bionic limbs. Gherardini *et al.* have now developed a myokinetic interface involving the implantation of magnets within muscle groups of the residual limb of a transradial amputee and a prosthesis device controlled wirelessly. Muscle deformation due to voluntary contraction was harnessed for dexterous bionic hand control through a direct control strategy and with the aid of a pattern recognition algorithm, enabling the user to carry out functional tasks such as picking up and grasping fragile objects as well as tying shoelaces. —Amos Matsiko